Experiments on Wideband Through the Wall Imaging[1]

Ronald Dilsavor[a], William Ailes[b], Paul Rush[c], Fauzia Ahmad[d], William Keichel[a], Gerard Titi[e], Moeness Amin[d]
[a]AFRL/SNAS, Bldg 620, 2241 Avionics Circle, Wright-Patterson AFB, OH 45433-7321
[b]General Dynamics Advanced Information Systems, 947 Mearns Road, Warminster, PA 18974
[c]Naval Surface Warfare Center, 4700 South Broad Street, Philadelphia, PA 19112-5083
[d]Villanova University, Center for Advanced Communications, Villanova, PA 19085
[e]DARPA IXO, 3701 N Fairfax Drive, Arlington, VA 22203-1714

ABSTRACT

The Center for Advanced Communications (CAC) at Villanova University has conducted several preliminary through-the-wall imaging experiments and collected real data on different settings behind the wall using a newly-integrated RF instrumentation suite. The full-polarization, 2D aperture data measurements are taken using an Agilent network analyzer, Model ENA 5071B, implementing a step frequency waveform over a 2-3 GHz frequency range. The room imaged is a typical computer lab that has been lined with radar absorbing material. Three different arrangements of the room's contents are considered: empty scene, calibration scene, and populated scene. The empty scene allows measurement of the noise/clutter background and supports coherent subtraction with the other two scenes. The calibration scene contains isolated reflectors that may be used to determine a fully-polarimetric radiometric calibration solution for the experimental system. The populated scene contains a number of common objects such as a phone, computer, tables, chair and filing cabinet. In addition, a jug of saline solution has been added to crudely approximate a human. Each scene is imaged with and without a wall. The wall is composed of plywood and gypsum board on a wood frame. The antennas are mounted on a 2D scanner that moves the antennas along and adjacent to the wall and is controlled by the network analyzer. Two additional antennas are fixed to the scanner frame and act as bistatic receivers. The paper provides a detailed description of the RF system and experimental conditions and provides a quick look at collected data products. The data measurements, technical details on collection instrumentation, auxiliary measurements, and scene truth data will be made available starting in April 05 to download from the Villanova CAC website at http://www.engineering.villanova.edu/cac/TWRI-experiments.

Keywords: Through the Wall Imaging, Beamforming, Near Range Imaging, 3D Imaging, Imaging Through Dielectric Media, Public Release Data Set, Full Polarization, Wideband, Stepped Frequency Waveform, Bistatic

1. INTRODUCTION

With recent advances in both algorithm and component technologies, THrough Wall At RF (THWARF) is emerging as an affordable sensor technology supporting a variety of applications. Current applications of the technology, in particular those utilizing ultra-wideband (UWB) technology, are limited to such applications as emergency rescue and fire fighting [1] as governed by Part 15 Subpart-F of FCC Telecommunications Act [2].

Due to the complexities associated with the development of successful through-wall systems, commercial offerings of through-wall technology have been limited to date. THWARF sensing presents numerous technical challenges including a less-than-cooperative propagation environment, (often) ad hoc antenna deployments, and inhomogeneities and non-stationarities in both the background environment and target set. While there are reported successes related to through-wall sensing [3][4], numerous improvements can be envisioned for future systems. Although existing technologies have proven successful in some environments, that success is not guaranteed everywhere. Differences in construction techniques, available materials and expertise, and personal and cultural preferences can lead to substantially different EM environments, and performance can vary substantially from one building / region to another. Finally, specific to RF techniques, lower frequencies are generally preferred due to their favorable propagation

[1] Distribution Statement A. Approved for public release, distribution unlimited. Cleared by DARPA [3/7/2005]. DISTAR case 4357.

(attenuation and backscatter) characteristics. Unfortunately, there isn't a lot of bandwidth at lower frequencies. Hence, the range resolution of these systems is limited. In addition, the spectrum is well occupied by legacy systems with authorization to use the spectrum. As a result, there are significant frequency allocation and RFI (radio frequency interference) issues that must be overcome if successful operation is to be routinely achieved.[2] In short, THWARF sensing is a difficult proposition.

While through-wall addresses a number of practical problems, it is dual-use with obvious military applications. This, combined with intellectual property issues, tends to reduce the incentive to collaborate and socialize ideas, and generally stifles innovation in the field. It is the authors' contention that system development suffers and sub-optimal solutions emerge from less-than-systematic development and evaluation processes. In addition, there appears to be a fair duplication of effort due to a lack of socialization both on the commercial and military sides.

Although many of the institutional problems will likely never be overcome, development efforts can be improved by standardizing at some levels. At present, it is difficult to compare and evaluate systems in a consistent manner. The community lacks agreed upon performance metrics and standardized test scenes. In addition, unlike other communities such as speech [5], adaptive array processing [6][7], and automatic target recognition [8][9][10], the through-wall community lacks benchmark datasets. Benchmark datasets could facilitate the standardization of performance metrics and the development and comparison of algorithms and system concepts.

In this paper, in conjunction with companion datasets to be distributed by Villanova, we attempt to reduce some of the entropy, that is, increase the coherence of algorithm and technology development and evaluation relevant to TWARF sensing. We acknowledge that the datasets provided represent a modest effort, and hope that others will consider both natural and novel extensions to our work. The collections described here are among the first taken by the recently integrated instrumentation suite at Villanova. Researchers there are just beginning to analyze the data.

The datasets were collected at Villanova as part of ongoing efforts in this field by the University as supervised by the Defense Advanced Research Project Agency (DARPA) and in collaboration with the Air Force Research Laboratory (AFRL). The datasets were collected in general engineering work space at the University, but with consideration given to the collections undertaken. The datasets include free-space and through-wall collections with and without calibration targets and a complex background that includes office furniture and laboratory equipment. Data is collected with largely off-the-shelf equipment including an Agilent network analyzer. Attributes of the data include a 1 GHz waveform bandwidth centered at 2.5 GHz, a two-dimensional synthetic aperture, 49" on a side, with a sample spacing of 0.875" on a square grid. In addition, the data is fully polarimetric. More importantly, the data may be radiometrically calibrated and the scenes are well ground-truthed. The datasets are admittedly sterile and somewhat naïve as they relate to problems encountered in real-world applications. The datasets represent a necessary compromise given the potential military utility of the technology.

The rest of this paper describes the collections and datasets in greater detail. The paper is organized as follows. Section 2 describes the RF system and mechanical scanner employed to collect the data. Section 3 describes the constituent parts that are "assembled" to produce the scenes. Section 4 describes the scenes and the collection plan. Section 5 offers a preview of the data including some preliminary results. In Section 6 we offer observations and lessons learned. Section 7 presents our conclusions.

2. RF SYSTEM DESCRIPTION

2.1. RF Equipment

Figure 1 shows a block diagram of the Villanova RF measurement system consisting of a network analyzer which transmits a stepped frequency waveform, cables, antennas, 2D antenna positioning system, and computer controller.

[2] While FCC Part 15 allows for the use of very low power UWB radiation, the UWB sources are permitted on a not-to-interfere basis with authorized users of the spectrum. In addition, UWB systems covered by Part 15 rules have no recourse against RF interference received by authorized users of the spectrum.

2.1.1. Network Analyzer

A standard 4-port network analyzer calibration procedure was followed to effectively eliminate directivity error, crosstalk, source match error, load match error, frequency response reflection tracking error and frequency response transmission tracking error. When completed, the phase reference point is normalized to the feed point of each antenna which corresponds to z=0 in our 3D coordinate system.

Data was collected on two separate channels to optimize the tradeoff between collection time and system sensitivity. Each channel used a 2.0-3.0 GHz frequency band and a 5 dBm transmit power. However, as shown in Table 1, cross-port parameters S12, S13, etc. were measured using a 70 kHz IF bandwidth (IFBW) whereas co-port parameters S11 and S22 were measured using a 7 kHz IFBW (Note that S_{ij} is the set of data obtained using i-th port as the transmitter and j-th port as the receiver). The wider IFBW speeds up data collection by reducing the length of the IF digital filter (shorter pulse matched filter) whereas the narrower IFBW used for the co-ports S11 and S22 helped to compensate for a 20dB directional coupler loss seen by the co-ports at the expense of additional collection time needed to implement the narrower digital filter.

Table 1. Channel Parameters.

Channel #	IF Bandwidth (kHz)	S-Parameters Measured
1	70	S12, S13, S14, S21, S23, S24, S32, S34, S42
2	7	S11, S22 (true monostatic measurements)

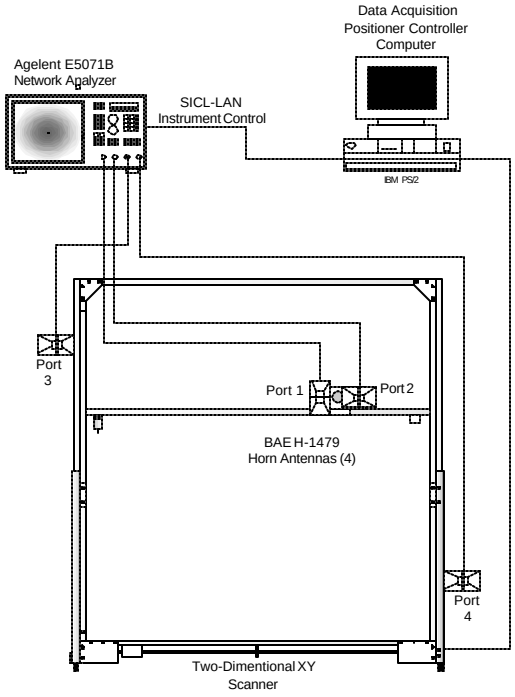

Figure 1. System Block Diagram.

2.1.2. RF Cables

The four coaxial cables that connect the network analyzer to the antennas were 20 ft in length and had a nominal loss of 2.5dB. The cables are further described in Table 2.

2.1.3. Antennas

The Port 1 antenna of Figure 1 is oriented for horizontal polarization whereas the remaining three antennas are oriented for vertical polarization. The antennas have approximately 10dB gain and, when oriented for horizontal polarization (as in Port 1), they have 45° azimuth 3dB beamwidth and 60° elevation 3dB beamwidth. Additional details are provided in Table 3. Figure 2 shows the azimuth and elevation antenna beam patterns for the antenna when oriented for horizontal polarization.

Table 2. Coaxial Cable Specification.

Manufacturer	Micro-Coax
Part No.	UFA21OA-0-2400-704704
Length	20 ft
Serial Nos.	Port 1: 209075-009, Port 2: 209075-008, Port 3: 209075-007, Port 4: 209075-010
VSWR	< 1.07:1 between 2.0 - 4.0 GHz
Cable Loss	2.0 dB at 2.0 GHz, 3.0 dB at 4.0 GHz

2.1.4. System Sensitivity

Next we calculate the signal-energy-to-noise-spectral-density ratio for the system:

$$S/N = \frac{P_{ave}G_t}{4pR^2}\cdot\frac{s_t}{4pR^2}\cdot\frac{G_r l^2}{4p}\cdot\frac{T_{CPI}}{kTFL_c L_w L_{xx}}$$

$$\approx 83(dB/sm) + s_t(dBsm) - L_w(dB) \quad \text{at 10 ft range for measurement of S11 and S22}$$

$$\approx 98(dB/sm) + s_t(dBsm) - L_w(dB) \quad \text{at 10 ft range for the other measurements}$$

where $P_{ave} = -25dBW$, $G_t = G_r = 9.9dB$, s_t is the radar cross section of the scattering object, $l^2 = -18.4dBsm$ for 2.5GHz center frequency, T_{CPI} is the coherent integration time in seconds and will be further discussed in a moment, $(4p)^3 = 33dB$, $R^4 = 19.4dBm^4$ at 10 ft mid-range, $L_c = 5dB$ is the 2-way cable loss (see Table 2), L_w is the wall loss, $L_{xx} = 20dB$ for S11 and S22 measurement (loss through directional coupler) and $L_{xx} = 0$ dB otherwise, and $kTF = -228 + 24 + 4 = -200$ dB W/Hz is the noise spectral density in the received signal. Since the network analyzer receiver noise figure was not available from Agilent at the time of publication, we have assumed without verification that it is $F = 4$ dB. Based on advice from Agilent technical support, we roughly estimate $T_{CPI} \approx T_{sweep}/2$ where T_{sweep} is the wall clock time to step through all 201 frequencies. For measurement of S11 and S22, $T_{CPI} \approx -16.4$ dBs, otherwise, $T_{CPI} \approx -20.5$ dBs. Though this equation is a rough approximation, we see that for low-loss walls and even low-cross-section targets we still expect substantial S/N. Hence, we expect range profiles to be limited by sidelobes, equipment stabilities, and perhaps clutter background.

2.2. Boresight Two-Dimensional X-Y Field Probe Scanner with Antenna Configuration

The Damaskos, Inc. Field Probe Scanner model 7X7Y, shown in Figure 3 was used for the experiment. Figure 3 also shows the coordinate system that is used throughout the paper. The center of the 2D aperture is located at X=0, Y=0, Z=0. The positive Z axis points into the room to be imaged and Z=0 corresponds to the plane containing the antenna phase centers. The scan area was configured to allow both the horizontally and vertically polarized antennas (port 1 & 2, respectively) to scan a zone 49" square. This was selected to provide roughly 6" crossrange resolution at midrange (10ft range). Due to the 10.5" horizontal separation between the Port 1 and 2 antennas, the X-axis (horizontal) scan was increased to 59.5" to provide total coverage of the scan area for each antenna. Data was collected at a total of 3933 discrete points, each point was separated by .875" in both the vertical and horizontal planes. At each of the 3933 points data was collected at 201 frequencies between 2.0 and 3.0 GHz (5 MHz steps). The stationary antennas (Ports 3 and 4) were mounted at a 10° angle; Port 3 downward, Port 4 upward to minimize multipath reflection from the ceiling and floor.

Table 3. Antenna Specifications.

Manufacturer	BAE Systems
Part No.	H-1479
Freq. Range	1.0 – 12.4 GHz
Serial Nos.	Port 1: 929, Port 2: 777, Port 3: 928, Port 4: 931
VSWR	< 1.8:1 for 2–3 GHz
Cable Loss	• 2.0 dB at 2.0 GHz • 3.0 dB at 4.0 GHz
Typical Boresight Gain	• 9.1 dB at 2.0 GHz • 9.9 dB at 2.5 GHz • 10.2 dB at 3.0 GHz
Typical 3 dB BW (Vertical)	• 60° at 2.0 GHz • 60° at 3.0 GHz
Typical 3 dB BW (Horizontal)	• 50° at 2.0 GHz • 40° at 3.0GHz

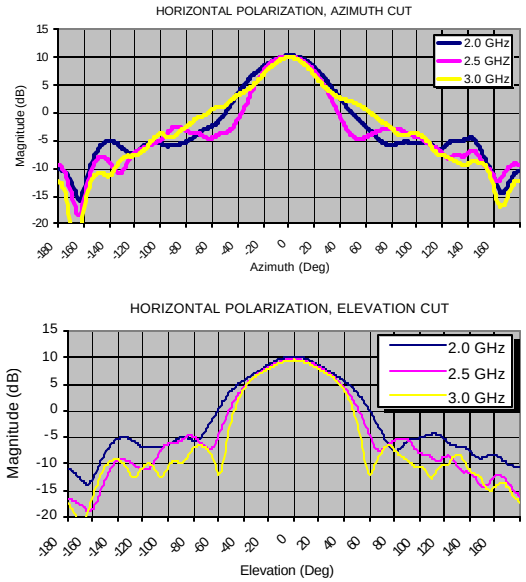

Figure 2 Antenna Beam Patterns.

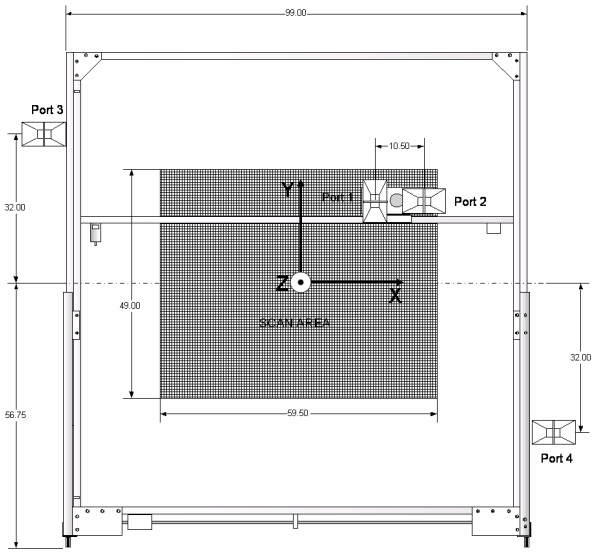

Figure 3. Damaskos, Inc. FieldProbe Scanner Model 7X7Y with antennas. Measurements in inches. Note XYZ Coordinate System.

3. SCENE CONSTITUENTS

3.1 Room Description

A 25' x 25' section of an engineering laboratory was selected for the experiment. The overall ceiling height of the space is approximately 12', however, the space incorporates exposed ventilation ducts and suspended lighting fixtures, which effectively reduce the overhead clear area to 9'. Precautions were taken by covering these potential reflectors with two inch laminated polyurethane foam sheet absorber. Additionally, due to the presence of some permanent equipment situated within the laboratory, 4' x 8' absorbing wall modules were constructed utilizing 18" pyramidal foam absorber. The wall modules were strategically positioned along the back wall and side areas to minimize the overall reflected energy present in the room. This configuration became the prototypical "empty scene" shown in Figures 7(a) and 8(a).

3.2 Wall Description

A typical residential exterior wall was selected for the test. A 12' x 8' wall segment was fabricated utilizing 2x4 wood studs placed on 16" centers. Exterior grade ¾" plywood was fastened to one side and ?" gypsum wallboard was applied to the other. See Figure 4.

(a) Wood Frame (b) Plywood Exterior (c) Gypsum Interior

Figure 4: Wall Construction.

The transmission coefficient of the wall for normal incidence was measured using the arrangement shown in Figure 5. Horn antennas 1 and 2 were placed on tripods on either side of the plywood-air-drywall wall at a distance of 51" each. Horn 1 was used to transmit a stepped frequency signal of 1 GHz bandwidth centered at 2.5 GHz and the complex amplitudes of the signal received by Horn 2 were measured and recorded. This experiment was repeated using the same exact setting with one exception; the wall was not present. The ratio of the two measurements was used to determine the transmission characteristics of the wall as a function of frequency.

Two sets of measurements were made to collect both HH- and VV-polarization data as shown in Figure 6. Note that transmission loss largely falls in the range 0-4 dB and is dependent on polarization. The transmission loss for vertical polarization is, on the average, slightly higher than that for horizontal polarization. We must point out that the 51" separation of the antennas from the wall is unique to this transmission measurement. The authors intend to repeat this measurement with the transmit and receive antennas close to the wall so as to emulate the conditions (shown in Figure 7(d)) in which our dataset is collected.

3.3 Available Reflectors

Table 4 lists the reflectors that were available to populate the scenes.

Table 4. Available Reflectors.

Calibration Reflectors	Other Scene Constituents
3" Seam Triangular Plate Trihedrals, RCS = -20.6dBsm*	Wooden Desk
6" Seam Triangular Plate Trihedrals, RCS= -8.5dBsm	Metal Table
12" Square Plate Dihedrals , RCS = 11.3 dBsm	5-Drawer Filing Cabinet
12" Diameter Sphere, RCS = -11.4dBsm	Office Chair
Tophat, 5" cylinder width, 20" cylinder height, 28" circular ground plane diameter	Metal pipe, 4' long, 2" diameter
	5 Gallon jug filled with salt water
* Used PO approximation, expect inaccuracy for the small 3" trihedrals	Computer with monitor

4. SCENE DESCRIPTIONS

Three distinct scenes were measured; empty scene, calibration scene, and populated scene. Each scene was measured both with and without the intervening wall. The scenes were carefully laid out and documented in XYZ coordinates.

4.1. Empty Scene

This scene was designed and measured with only the absorbing wall modules present in the test area. The overhead light fixtures and exposed ventilation ducts were covered with laminate sheet absorber as shown in Figure 7(a).

Empty Scene with Wall: In this configuration the test environment remained the same as the "Empty Scene" with the exception of the introduction of the 12' x 8' wall segment. The wall was positioned ½" downrange from the front face of the antennas as shown in Figure 7(d).

4.2. Calibration Scene

This scenario consisted of the empty scene modified to incorporate a series of calibration reflectors. These reflectors with known RCS values were methodically positioned within the scan zone. The measured scene consisted of three 12" dihedrals, three 3" trihedrals, one 6" trihedral, one 3" diameter cylinder and one 12" diameter sphere. Each target was mounted at a unique range bin and angular displacement as shown in

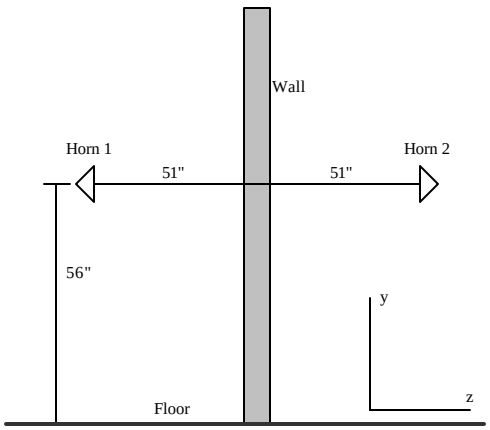

Figure 5 Experimental set-up for measurement of the transmission characteristics of the wall.

Figures 7(b), 8(b), and 9(a). The three dihedrals were tilted at 0°, 22.5°, and 45° about the radar line of sight. These tilted dihedrals and the 6" trihedral are there to enable full polarization radiometric calibration of the data [11][12].

Calibration Scene with Wall: In this configuration the test environment remained the same as the "Calibration Scene" with the exception of the introduction of the 12' x 8' wall segment. The wall was again positioned ½" downrange from the front face of the antennas as shown in Figure 7(d).

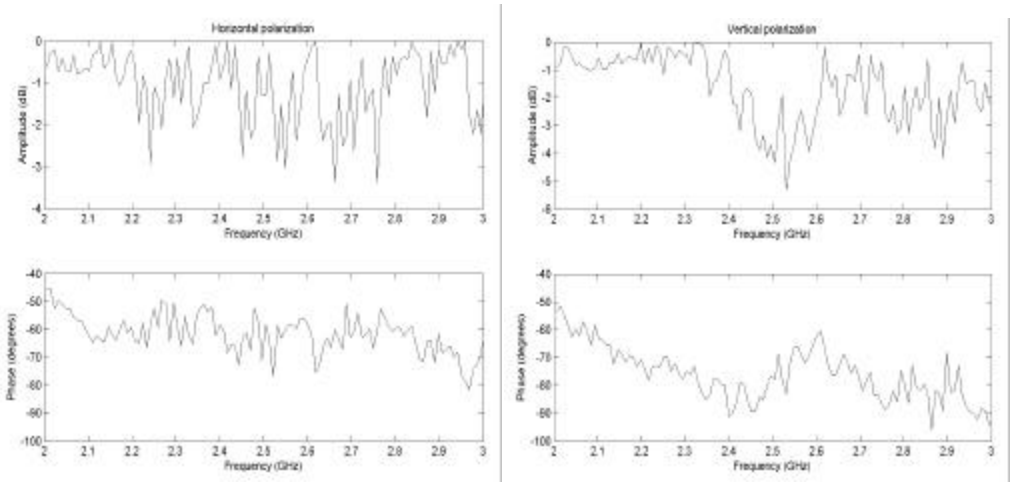

(a) HH pol (b) VV pol

Figure 6. Wall transmission measurements with antennas placed 51" from wall. Measurements to be repeated with antennas ½" from the wall as in Figure 7(d).

4.3. Populated Scene

This scenario consisted of the empty scene modified to incorporate a combination of typical office furniture and canonical reflectors. The scene was populated with one wooden desk, one metal workbench, one desk chair, one 5-drawer filing cabinet, one PC setup consisting of a CPU and monitor, one telephone, one 5-gallon jug of saline, one 4-foot pipe with 2-inch diameter, three 6" trihedrals and two 3" trihedrals as shown in Figures 7(c), 8(c), and 9(b).

Populated Scene with Wall: In this configuration the test environment remained the same as the "Populated Scene" with the exception of the introduction of the 12' x 8' wall segment. The wall was positioned ½" downrange from the front face of the antennas as shown in Figure 7(d).

Floor plans for the three scenes are shown in Figure 8 and layout dimensions are captured in Figure 9.

(a) Empty Scene (b) Calibration Scene

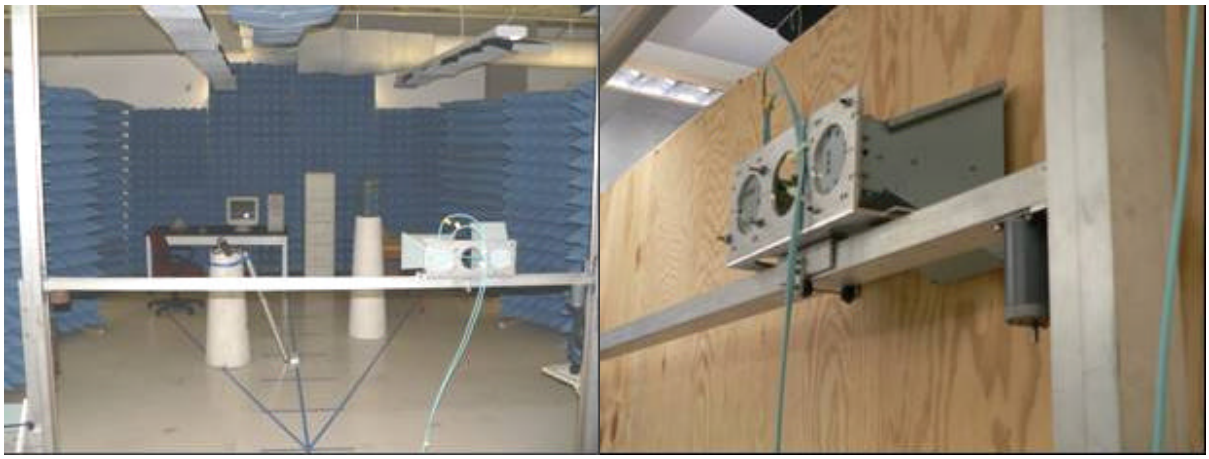

(c) Populated Scene (d) Antenna-Wall Positioning

Figure 7. Scene Photos.

5. DATA PREVIEW

5.1. Selection of Unambiguous Range

The maximum unambiguous range, R_u and the frequency step size, Δf , of the stepped-frequency signal are related by $R_u = c/2\Delta f$. The distance from the array baseline to the back wall in the lab is 25 ft. In order to determine the maximum unambiguous range to allow for multiple bounces off of the front, side, and back walls, we carried out the following experiment. We set the step size to 5 MHz, which corresponds to a large 30m one-way unambiguous range and averaged the complex amplitude data obtained from 1000 sweeps, for the empty scene, with the scanner carriage at the center of the scanning area. Sweep averaging was carried out to reduce the random noise in the measurements. Figure 10 shows the round-trip range profiles for S11, S22, and S23 measurements. We note that there are significant returns from round-trip ranges between 45 and 55m for both S11 and S22 measurements. Further investigation is required to determine whether these originated from the scene or are artifacts of wideband pulse synthesis. We, therefore, retain the 5 MHz step size and thereby the 30m maximum one-way unambiguous range for our experiments. The number of frequency steps required to synthesize the 1 GHz stepped-frequency signal is 201.

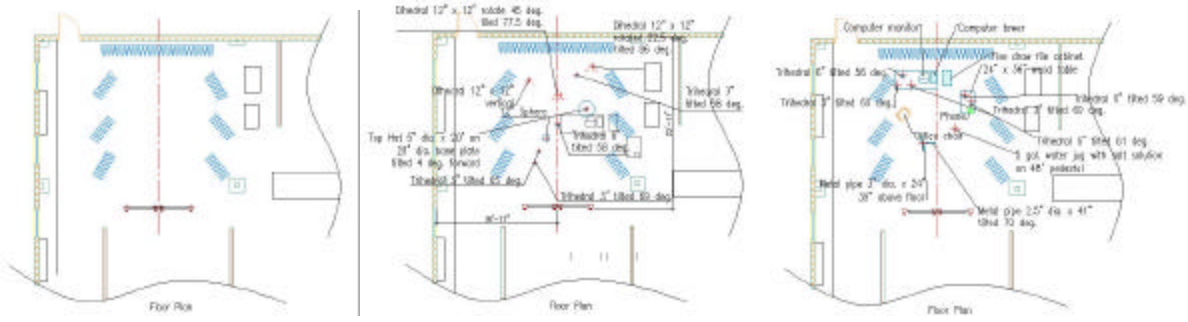

(a) Empty Scene (b) Calibration Scene (c) Populated Scene

Figure 8. Floor Plans.

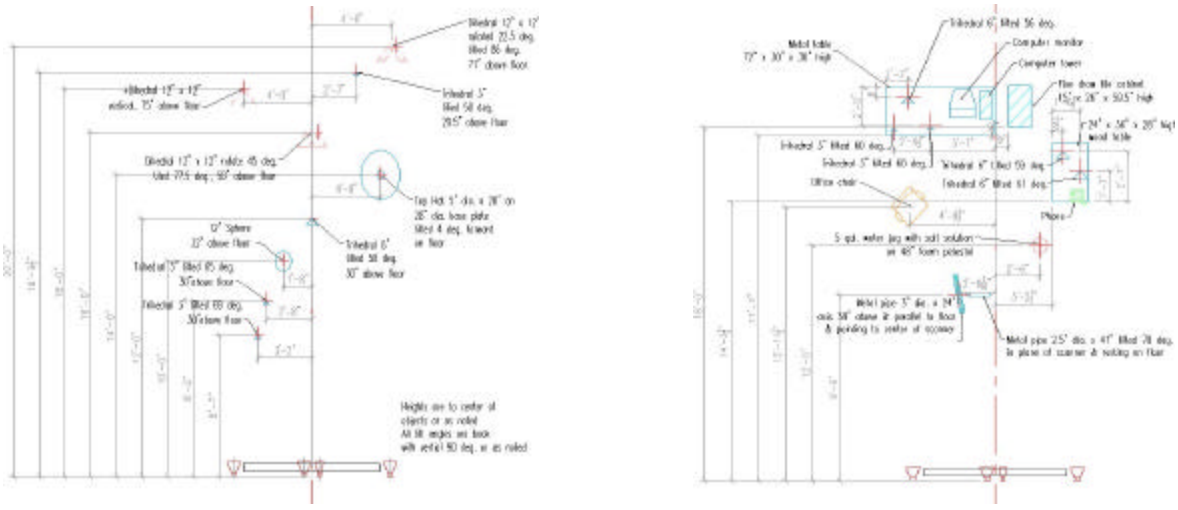

(a) Calibration Scene **(b) Populated Scene**

Figure 9: Scene Dimensions

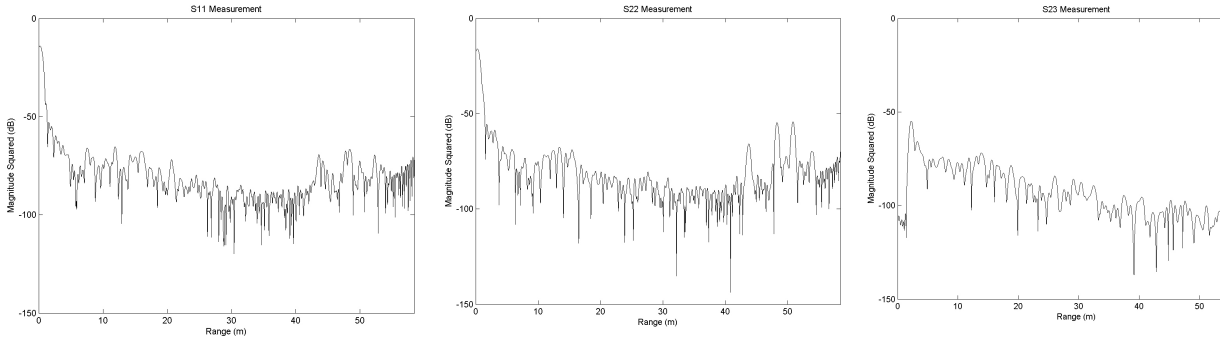

Figure 10: Empty Scene round-trip range profiles for S11, S22, and S23 measurements. 5MHz steps.

5.2. Synthetic Aperture Beamforming [13]

Consider a single transmitter and a single receiver, which are to be used to synthesize a *P*-element transmit and a *Q*-element receive array, both located in the XY-plane. The region to be imaged is located along the positive z-axis. Let the transmitter, placed at the *p*-th transmit location $\mathbf{x_t(p)}=(x_t(p), y_t(p))$, illuminate the scene with a sequence of K monochromatic signals spanning the desired bandwidth (stepped-frequency wideband signal consisting of K frequency steps). The complex amplitudes of the returns are measured and stored by the receiver at the *q*-th receive location $\mathbf{x_r(q)}=(x_r(q), y_r(q))$. This process is repeated, with the transmitter at the *p*-th location, until all the *Q* receive locations have been used sequentially. The above data measurement process is then repeated by sequential use of the *P* transmit locations.

For a single point target located at $\mathbf{x}=(x, y, z)$, the corresponding *KPQ* outputs are processed as follows and the beamforming process is also depicted in Figure 11. The region of interest is divided into a finite number of voxels in downrange and both cross-range directions. The complex amplitude image value for the (l,m,n)-th voxel located at $\mathbf{x_q}=(x_q, y_q, z_q)$ is obtained by applying frequency-dependent phase delays and weights to the measured data, and combining the results as per the following equation

$$I(l,m,n) = \sum_{p=1}^{P}\sum_{q=1}^{Q}\sum_{k=1}^{K} w_{tp}\, w_{rq} F(w_k) R_{pq}(w_k) \exp(\, jw_k t_{\,pq}(l,m,n))$$

where w_{tp} ,w_{rq} are the weights applied to shape the beam, $R_{pq}(w_k)$ is the measured complex amplitude of the return when the transmitter is at the p-th location and the receiver is at the q-th location, $F(w_k)$ are the weights applied to synthesize a desired pulse spectrum, and $t_{pq}(l,m,n)$ is the focusing delay applied to the output of the q-th receiver when the transmitter is at the p-th location. The focusing delay is given by

$$t_{\,pq}(l,m,n) = (d(\mathbf{x_t(p)}, \mathbf{x}) + d(\mathbf{x_r(q)}, \mathbf{x}))/c$$

where $d(\cdot,\cdot)$ is the Cartesian distance between two position vectors and c is the propagation speed. This delay synchronizes the arrivals at different receive locations for the same voxel, and as such allows coherent imaging of the scene. Unlike the focusing delays, the weights, w_{rq} and w_{tp}, are independent of the voxel location $\mathbf{x_q}$, and serve to design the system point spread function according to desired specifications.

The process, described above, is performed for all voxels in the region of interest to generate the composite image of the scene. The general case of multiple targets can be obtained by superposition of target reflections.

5.3. Empty Scene

Figure 12 shows the S11, S12, and S23 range profiles for one of the transmitter/receiver pair locations, for both without and with-the-wall empty scene. The horizontal axis is round-trip range in feet and the vertical axis is the received power relative to the 5dBm transmit signal. Range profiles are generated using an inverse Fourier transform of the complex amplitudes of all 201 monochromatic signals. The profiles without the wall (top row) clearly show mutual coupling effects at short range whereas those for with-the-wall case indicate the returns from the front and back faces of the wall as well.

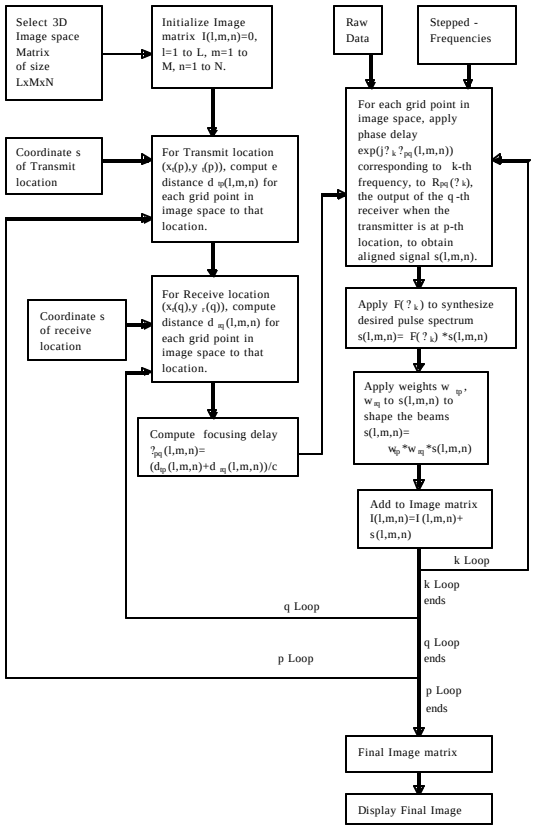

Figure 11. Block diagram of the beamforming process.

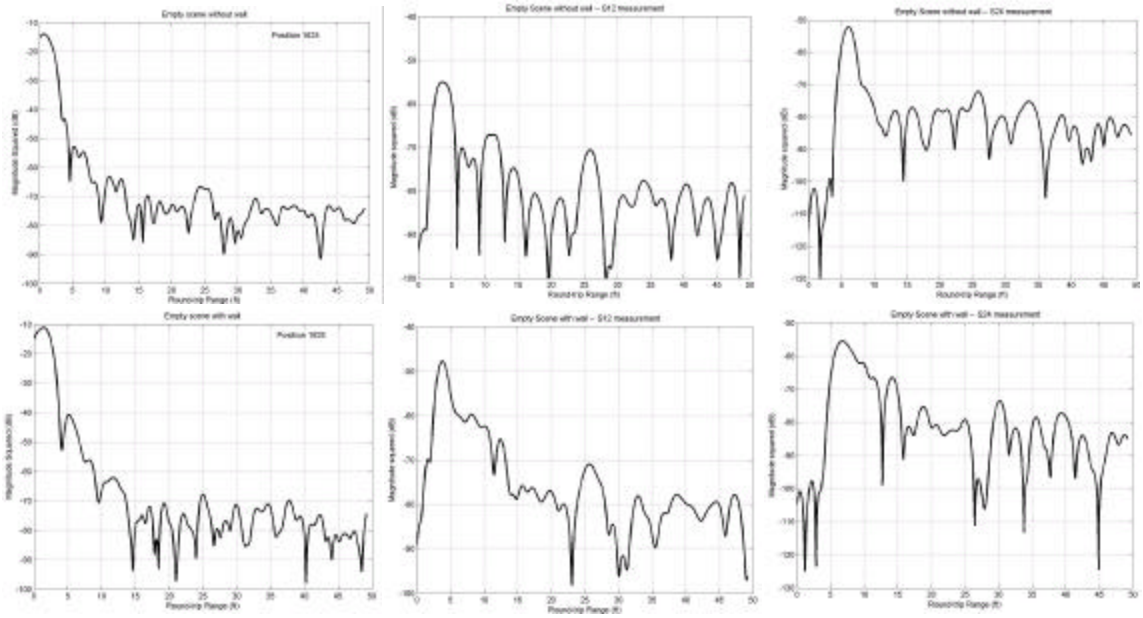

Figure 12: Empty Scene range profiles for the S11, S12, and S23 measurements with antenna 1 positioned at the origin (center of the scanning plane). Top row corresponds to empty scene without wall and the bottom row represents the empty scene with the wall. Note the differences in the Y-axis scales on these plots.

5.4. Calibration Scene

The empty scene measurements are subtracted from the corresponding calibration scene measurements for clutter reduction. This final data after clutter subtraction was used for range and cross-range processing of the calibration scene. Figure 13 shows the range profiles of the S11 (horizontal polarization) stepped-frequency data, before and after background subtraction, for one of the transmitter/receiver pair locations in the presence of the wall. We can see from Figure 13 that the returns from the targets (for round-trip range values between 13 and 40 ft) are more prominent after background subtraction. Note that we are unable to resolve in range the vertical dihedral and the 3″ trihedral tilted 58 degrees since they are separated in range by roughly 7 inches.

Figure 14 shows HH polarization horizontal X-axis cuts through the 3D volume at various downranges and heights. The beamformer has accurately located all the targets starting from the nearest 3″ trihedral to the 12″ dihedral farthest from the array. Note that the vertical dihedral and its neighboring trihedral, unresolved in range, have been successfully resolved in cross-range X and height Y.

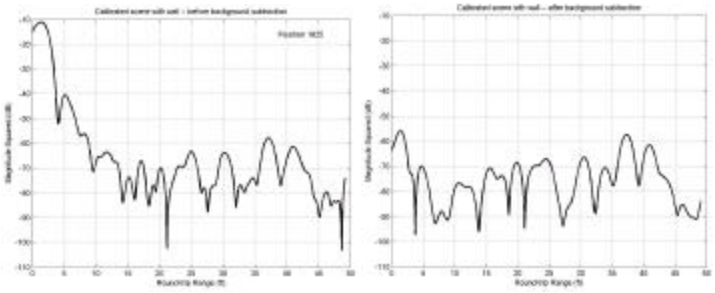

Figure 13: HH polarization range profile for the calibration scene with wall before and after background subtraction.

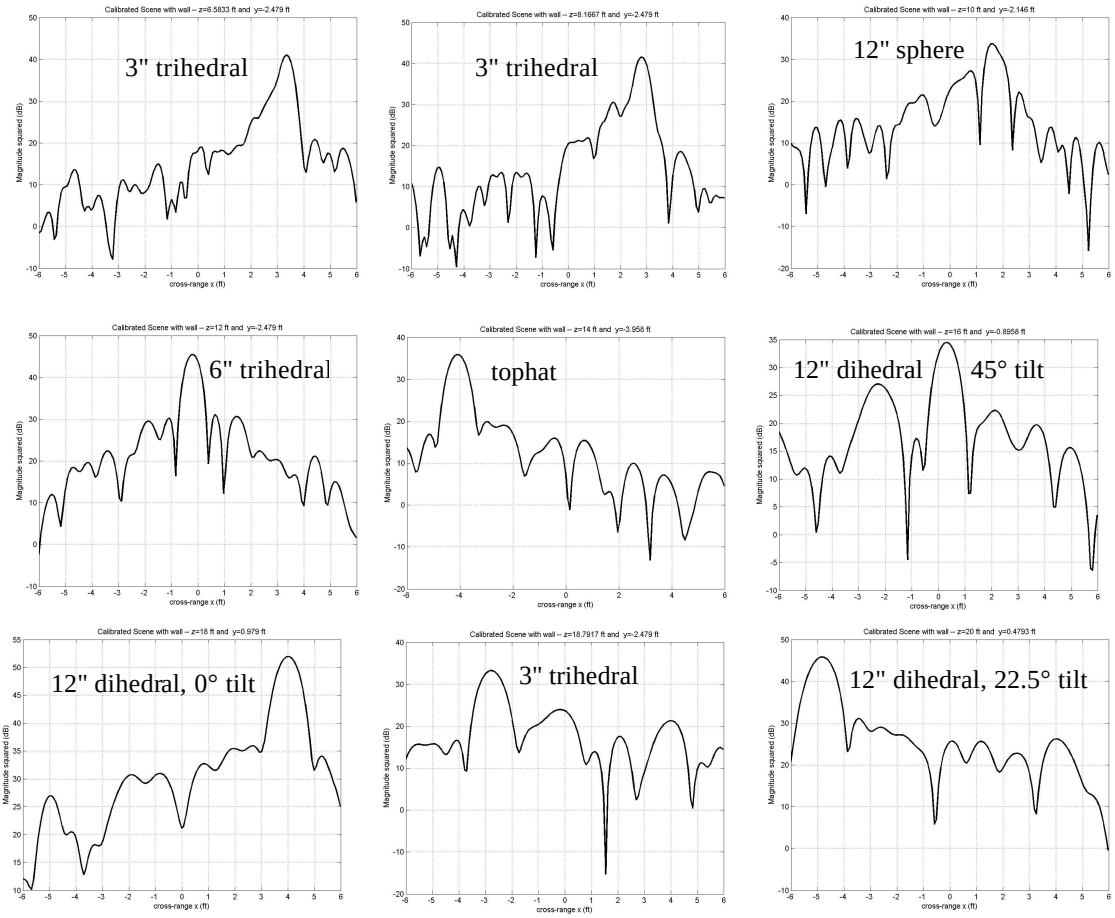

Figure 14. Calibration Scene with wall. HH polarization X-axis slices at various (range Z, height Y) values. The plots represent, from top left, the targets tabulated in Figure 9(a) starting from the nearest to the farthest from the array.

5.5. Populated Scene

The empty scene with wall measurements were subtracted from the populated scene with wall measurements for clutter reduction. This final data, after clutter subtraction, was used for range and cross-range processing of the populated scene Figure 15 shows the range profiles of the S11 stepped-frequency data, before and after background subtraction, for one of the transmitter/receiver pair locations in the presence of the wall. We can see from Figure 15 that although the background subtraction has been carried out, there is still residual clutter present due to interaction of the targets with the environment. Also, not all targets are resolvable in range.

Figure 16 shows the X-axis slices at various downrange Z and height Y values for the populated scene. We note that the two pipes are barely resolvable in cross-range at 39 inches height. Also, in the bottom right plot in Figure 16, we cannot differentiate between the returns from the computer and the trihedral on the metal desk for 30 inches elevation. On the other hand, the filing cabinet has

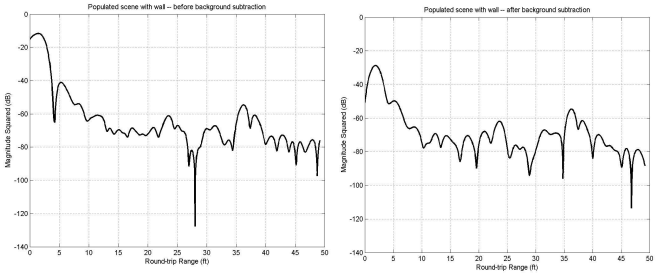

Figure 15: HH range profile for the Populated Scene with wall before and after background subtraction.

been correctly located. We further observe that if resolvable, the targets are accurately localized by the beamformer. However, especially for targets at downrange beyond that of the metal pipes, the X-axis slices show unexplained peaks of strengths comparable to the objects of interest. Further investigation is required to determine if these unwanted signals are due to multi-path (because of reflection off the floor etc.) or because of target interaction with each other.

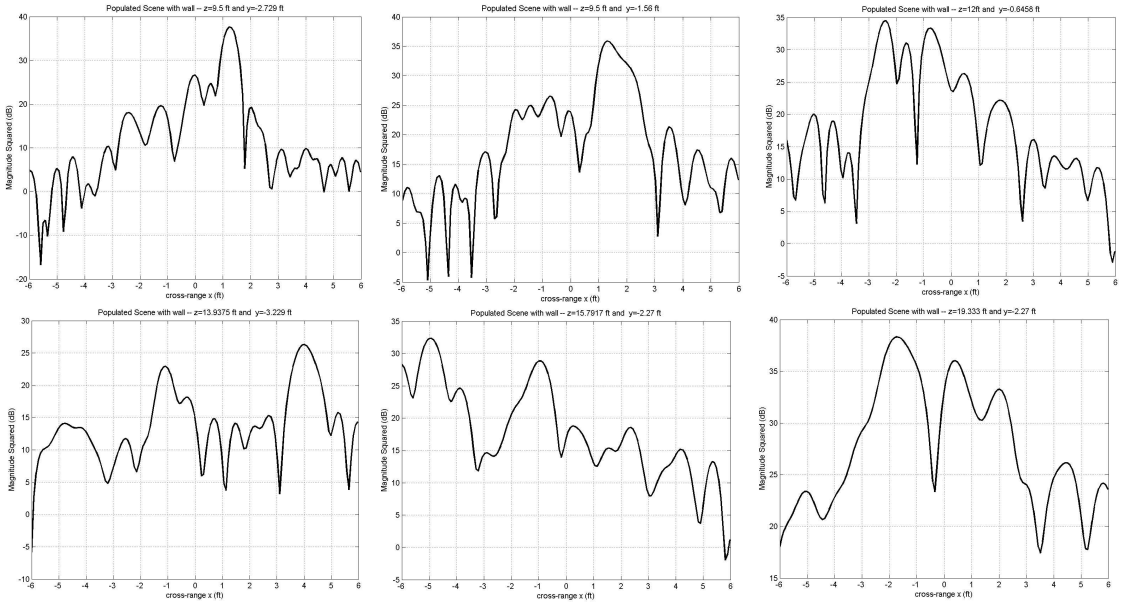

Figure 16: HH polarization X-axis slices at various (downrange Z, height Y) values for the populated scene with wall. From top left: Metal pipe tilted 70°, both metal pipes at 39 inches above the ground, salt water jug 50 inches above the ground, chair, 6^2 trihedral tilted 61° on wooden table, filing cabinet plus computer plus 6^2 trihedral on metal desk.

6. OBSERVATIONS AND LESSONS LEARNED

A rich dataset with spectral, spatial, propagation, and scene diversity has been assembled and will be made available to researchers interested in through-wall applications. The collections are among the first taken by the recently integrated instrumentation suite at Villanova. Researchers there are just beginning to analyze the data. Initial results suggest that objects are generally and clearly visible in beamformed outputs. However, as suggested in Section 5.1, there are as yet unexplained signals in the dataset. This isn't unexpected. Because of the dynamic ranges of the scenes, the resulting environment is quite complicated, despite our efforts to simplify it. These unexplained features may prove to be real or equipment-related artifacts, but likely represent interesting opportunities for researchers in either case.

During the course of the collection and the composition of this paper we have identified certain limitations in the dataset as it exists and will attempt to back-fill as time and resources permit. Some ways to improve on the current effort include

1. Produce a loop-back dataset to characterize equipment stability and to clearly assess the 3D impulse response of the system without the vagaries of imaging targets in the laboratory environment.
2. Produce a noise-only dataset to establish a noise floor reference against which other datasets and processed results can be compared.
3. More fully characterize the frequency responses of the antennas.
4. Implement a smaller frequency step size to better address extended returns.
5. Better characterize the through-wall attenuation by placing transmit and receive antennas closer to the wall.

Subsequent experiments will certainly reflect knowledge gained during the collection and documentation of this dataset.

7. CONCLUSIONS

We have conducted these THWARF measurements for the purpose of promoting disciplined research and comparison of results within the through-wall community. This data set enables exploration of near range 2D and 3D imaging techniques, focusing through intervening media, and polarimetric scene characterization. The sensed and auxiliary data has undergone public release and will be made available starting in April 05 via the Villanova Center for Advanced Communications (CAC) web site at http://www.engineering.villanova.edu/cac/TWRI-experiments. We expect to further investigate the remaining uncertainties in the data as described in Section 6 and to report on those results via the website. It is hoped that next year's SPIE Defense and Security Symposium will see a number of publications derived from this experiment. We look forward to a healthy interchange of ideas and results as we mature this important application area.

8. REFERENCES

[1] P. Withington, et al., "Enhanced Homeland Security with Advanced UWB Sensors", IEEE Microwave Magazine, September 2003.

[2] "FCC Part 15--Radio Frequency Devices", PART-15.ORG, 6 Mar 2005 <http://www.part-15.org/fcc/part15/15.htm>.

[3] "RadarVision", Time Domain Corporation, 6 Mar 2005, <www.radarvision.com>.

[4] "New Tracking and Communications Device Could Help Save Lives", Wireless Developer Network, 6 March 2005, <http://www.wirelessdevnet.com/channels/wireless/features/timedomain/>.

[5] "Benchmark Tests - NIST Spoken Language Technology Evaluations", National Institute of Standards and Technology, 6 March 2005, <http://www.nist.gov/speech/tests/>.

[6] G. W. Titi and D. F. Marshall, "The ARPA/NAVY Mountaintop Program: Adaptive Signal Processing for Airborne Early Warning Radar," *1996 IEEE International Conference on Acoustics, Speech and Signal Processing*, Atlanta, Georgia, May 7-10, 1996.

[7] "Mountaintop Radar", Rice University Signal Processing Information Base, 6 March 2005, <http://spib.rice.edu/spib/mtn_top.html#file1>.

[8] A. R. Wise, D. Fitzgerald, T. D. Ross, "The adaptive SAR ATR problem set (AdaptSAPS)", pp. 366-375, *Proc. SPIE*, vol. 5427, Algorithms for Synthetic Aperture Radar Imagery XI, April 2004.

[9] Kiranmai Naidu, Luke Lin, Visual-D Team, "Data dome: full k-space sampling data for high-frequency radar research", pp. 200-207, *Proc. SPIE*, vol. 5427, Algorithms for Synthetic Aperture Radar Imagery XI, April 2004.

[10] "SDMS Public Web Site", Air Force Research Laboratory Sensors Directorate, 6 March 2005, <https://www.sdms.afrl.af.mil/main.php>.

[11] M.W. Whitt, F.T. Ulaby, P. Polatin, and V.V. Liepa, "A general polarimetric radar calibration technique," *IEEE Transactions on Antennas and Propagation*, vol. 39, pp. 62-67, Jan. 1991.

[12] R. Barnes, "Polarimetric Calibration using In-Scene Reflectors", Project Report TT-65, MIT Lincoln Laboratory, 16 September 1986.

[13] F. Ahmad, G. J. Frazer, S. A. Kassam, and M. G. Amin, "Design and implementation of near-field, wideband synthetic aperture beamformers", *IEEE Trans. AES*, vol. 40, no. 1, pp. 206-220, Jan. 2004.